Journal of Inorganic Biochemistry 192 (2019) 1–6

Contents lists available at ScienceDirect

Journal of Inorganic Biochemistry

journal homepage: www.elsevier.com/locate/jinorgbio

A series of two-photon absorption organotin (IV) cyano carboxylate derivatives for targeting nuclear and visualization of anticancer activities

Qiong Zhang[a,*,1], Mingzhu Zhang[a,1], Hui Wang[a,c,1], Xiaohe Tian[b], Wen Ma[a], Lei Luo[d], Jieying Wu[a], Hongping Zhou[a], Shengli Li[a], Yupeng Tian[a]

[a] Department of Chemistry, Key Laboratory of Functional Inorganic Material Chemistry of Anhui Province, Anhui University, Hefei 230601, PR China
[b] School of Life Science, Anhui University, Hefei 230601, PR China
[c] Department of Chemistry, Wannan Medical College, Wuhu 241002, PR China
[d] College of Pharmaceutical Sciences, Southwest University, Chongqing 400716, PR China

ARTICLE INFO

Keywords:
Organotin
Two-photon absorption
Anticancer

ABSTRACT

Compared to organotin (IV) compounds with biochemical activity, two-photon absorption (2PA) organotin (IV) complexes for targeting nuclear with anticancer activities are rarely reported. Here, two novel 2PA organotin (IV) cyano carboxylate complexes (**C1Sn-1**, **C1Sn-2**) are synthesized and characterized. The two-photon absorption cross section values (δ) in the near-infrared region are significantly enhanced for **C1Sn-2** compared to **C1Sn-1**, thus developing for targeting nuclear by two-photon fluorescence microscopy (2PFM). **C1Sn-2** could specifically target nuclear DNA *in vitro*. The mechanism demonstrated that there are abundant hydrogen bond interactions between hydroxy group of **C1Sn-2** and DNA. The animal mode studies are first proposed that **C1Sn-2** displayed a certain anti-cancer efficiency with non-significant toxicity.

1. Introduction

Cancer is a major global problem and a leading cause of mortality [1]. Among several valid strategies at disposal for battling the disease, organic and inorganic compounds having high anticancer activity played pivotal role in chemotherapy. A variety of such anticancer drugs of organic genre, namely, taxol, podophyllotoxin, camptothecin, and so forth [2], and of inorganic genre, such as cis-diamineplatinum(II) dichloride (cisplatin) [3] and nanoparticles [4], were thus being routinely prescribed as a part of anticancer therapy. To explore more efficient and less costly anticancer agents, various organotin derivatives have been investigated for their structures and anti-proliferative properties against a number of cell lines [5–7]. For all the studied organotin compounds, the organotin carboxylates [8–12] are of the most intensively focused. Carboxylic acid as precursor offers a number of distinct advantages for its coordination ability, which serves as either a multidentate or a bridging building block in structural assemblies [13–19]. In our previous work, several organotin compounds derived from carboxylate acid ligands were reported [20–22]. Based on those carboxylate ligands, the resulting organotin compounds are reservoirs of many important properties including *in vitro* cytotoxicity and antitumor activities. In some cases, organotin (IV) derivatives have also shown acceptable anti-proliferative as new chemotherapy agents [23]. In this sense, the organotin carboxylates are like a chameleon in the organometallic area. However, our previous organotin (IV) derivatives are restricted to damage in cytosolic organelle (*e.g.* mitochondria and endoplasmic reticulum) [22], it should be noted that the anticancer compounds directly targeting genetic substances (*e.g.* DNA or RNA) in nucleus could be half the work with double results [24]. Compared to normal anticancer organotin derivatives, two-photon organotin agents apply longer exciting wavelength and low energy in the near infrared (NIR) region were used in order to display less photobleaching and deeper penetration depth (> 100 μm) [25–29].

Herein, two different classifications of second-substitute (Triphenyltin Hydroxide, tributyltin oxide) were used to synthesize a series of organotin (IV) complexes (**C1Sn-1**, **C1Sn-2**) based on carboxylate ligands. CN group with electron-withdrawing ability (Acceptor) has been extensively studied for interesting photophysical properties which should possess moderate two-photon action cross-sections favoring the application of two-photon fluorescence microscopy (2PFM) with deeper tissue-penetration and excellent resolution. Furthermore, CN group was used to improve the acidic ability which prone to deprotonation and might lead to high binding affinity towards metal ions [22]. Carboxylate unit might accelerate the penetration of

* Corresponding author.
E-mail addresses: zhangqiong.314@163.com (Q. Zhang), xiaohe.t@ahu.edu.cn (X. Tian), yptian@ahu.edu.cn (Y. Tian).
[1] These authors contributed equally to this work.

https://doi.org/10.1016/j.jinorgbio.2018.12.001
Received 8 June 2018; Received in revised form 28 November 2018; Accepted 2 December 2018
Available online 05 December 2018
0162-0134/

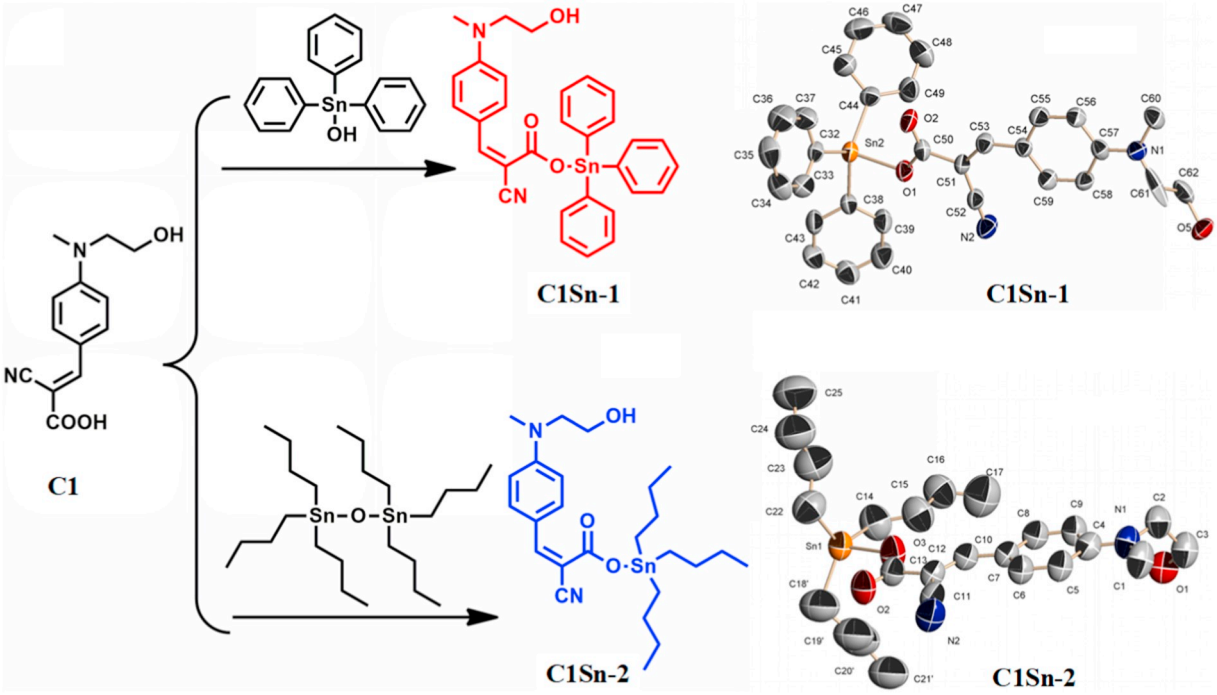

Scheme 1. Synthetic routes for **C1**, **C1Sn-1**, **C1Sn-2** and crystal structures of **C1Sn-1** and **C1Sn-2** (all H atoms were omitted for clarity).

the organotin(IV) derivatives across the cell membrane as well as aniline group with excellent planarity can connect with DNA based on insert model [30]. The two-photon absorption (2PA) activity was tuned by using styryl group due to its moderate π-conjugation system. Terminal −OH group might lead to good water-solubility and the formation of hydrogen bond with DNA to stable the molecule. Bis(tri-n-butyltin) oxide and triphenyltin hydroxide are low cost with high bioactivity and the alkyl chains can enhance the solubility of organotin (IV) complexes. Consequently, this is the first time that the 2PA organotin (IV) complex **C1Sn-2**, which present to image nuclear serve as a "light-switch" for DNA, have been displayed considerable inhibition towards solid tumor growth in a mouse model compared with commercially available anticancer clinical drug such as cis-platin.

2. Results and discussion

2.1. Synthesis and photophysical propertie

The detailed synthesis and characterization of organotin (IV) derivatives including **C1** and **C1Sn-1**-**C1Sn-2** used in this study were stated in the Supporting information (Scheme 1, Fig. S1–S3). Molecular structures were further confirmed by single-crystal X-ray diffraction analysis (Table S1–S3). Structural analysis revealed that the center Sn (IV) adopts distorted tetrahedron coordination geometry. The aniline group adjoins the Sn (IV) with the dihedral angle being 19.68° (**C1Sn-1**) and 8.17° (**C1Sn-2**), indicating that the favorable coplanar and abundant intermolecular hydrogen bonds in Sn (IV) complexes could result in higher delocalization in the π-electron conjugated system, which is necessary for nonlinear optical (NLO) response, as well as may be sensitive to nuclear of cells. Subsequently, their fluorescent properties have been investigated in details (Fig. S4–S5). **C1Sn-1** and **C1Sn-2** exhibited moderate fluorescence at ~434 nm than **C1** in DMSO-H_2O solution with the excitation at ~360 nm. The decreased spin-orbit coupling due to Sn atom can increase the energy level between the singlet and triplet excited states, causing the increase of fluorescence intensity. Different from the ligand **C1**, the complexes underwent a weak blue-shift with the emission around 439 nm, as a result of no significant permanent ground-state dipole moment in polar solvents [31], which were certified by computer-aided calculations (Fig. S6).

2.2. Two-photon absorption (2PA) cross sections and DNA binding experiments

The two-photon absorption properties were presented *via* open aperture *Z*-scan curves. It was found both **C1** and **C1Sn-1** show weak two-photon absorption activities. Interestingly, the two-photon absorption properties of **C1Sn-2** was apparently increased > 10 times rather than that of **C1** and **C1Sn-1** (Fig. 1(a) and Table S4), since the terminal n-butyl group can enhance the electron-donor character, converting **C1Sn-2** to a more polarized D-π-A unit in favor of intramolecular charge transfer (ICT) process affords them with stronger third-order nonlinear optical responses, which was in agreement with the above structural analysis. On the basis of the two-photon absorption spectra of **C1Sn-2**, we selected 730 nm as excitation wavelength, and 425–525 nm as collected range for two-photon biological imaging after evaluating their biological activity *in vitro*. (Fig. 1(b–d) DNA binding, Fig. S7–9). Upon increasing the concentrations of DNA, the absorption band at 260 nm displayed clear hyperchromicity, as defined by H % = 100 $(A_{free}\text{-}A_{bound})/A_{free}$, for the ICT band at 260 nm was found to be 53.6%. The intrinsic binding constant K_b of **C1Sn-2** with DNA was evaluated to be $8.69 \times 10^4\ M^{-1}$, which indicates the considerable intercalative binding intensity of **C1Sn-2** to DNA. The DNA binding property of **C1Sn-2** is also investigated *via* fluorescent measurement, based on the competitive binding between ethidium bromide (EB) and **C1Sn-2** with calf thymus dna (calf thymus dna (*ct*-DNA)). ethidium bromide (EB) molecules bound by calf thymus dna (calf thymus dna (calf thymus dna (*ct*-DNA)) gave strong fluorescence emission with maximum emission intensity at 597 nm. The fluorescent intensity of ethidium bromide (EB) was gradually decreased with increasing addition of **C1Sn-2**. K_{app} values was found to be $2.46 \times 10^5\ M^{-1}$, which indicates that there existed intercalative binding mode of **C1Sn-2** with DNA. This observation is in good agreement with the conclusions drawn from UV/vis titration studies [32]. Viscosity measurements were carried out to further clarify the nature of the interactions between **C1Sn-2** and DNA. The relative viscosity of calf thymus dna (calf thymus dna (*ct*-DNA)) bound with the **C1Sn-2** increased accompanied by increasing

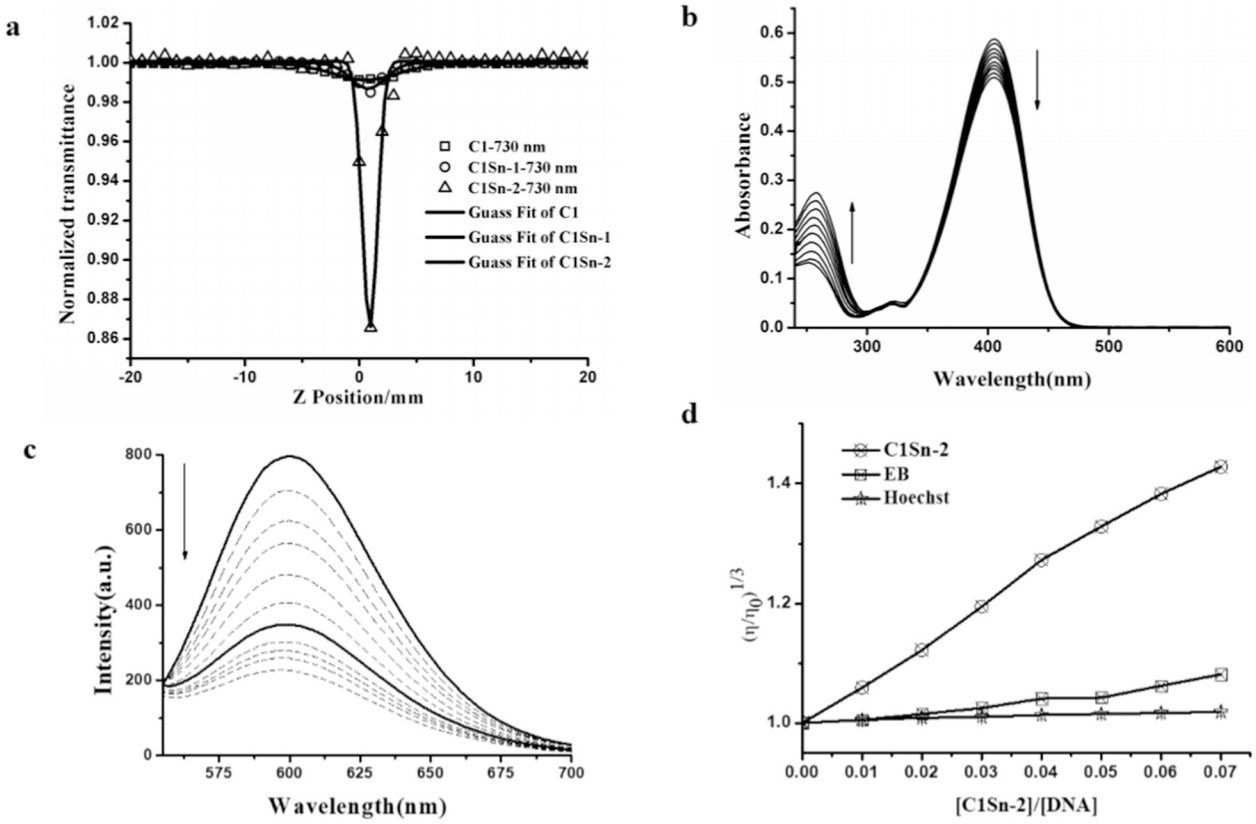

Fig. 1. (a) The open aperture *Z*-scan data at 730 nm for C1, **C1Sn-1**, **C1Sn-2** in DMSO-H_2O (c = 0.1 mM). The circle rings represent the experimental data and the solid curve is the theoretical data. (b) UV-vis absorption spectra of **C1Sn-2** (2 μM), in the absence and presence of increasing concentrations of calf thymus dna (calf thymus dna (*ct*-DNA)) (0–1.2 μM) in 50 mM Tris-HCl buffer (pH = 7.4, 50 mM NaCl). (c) Fluorescence spectra of ethidium bromide (EB) bound to DNA in the presence of **C1Sn-2** (0–16.7 μM). [EB] = 15 μM, [DNA] = 15 μM. The arrows show the intensity changes upon increasing concentrations of the complex. (d) The changes in the relative viscosities of DNA with increasing concentrations of **C1Sn-2** in buffer 50 mM NaCl. The total concentration of DNA is 50 μM.

complex concentration which is similarly to the behavior of some known DNA intercalators (ethidium bromide (EB), Hoechst) (Fig. 1d), indicating the classical intercalation of **C1Sn-2** to calf thymus dna (calf thymus dna (*ct*-DNA)). Combined with the results from the above-mentioned spectral analyses, the interaction between **C1Sn-2** and DNA is confirmed to be an intercalative binding mode.

2.3. Nuclear targeting function as anti-cancer property

Owing to the small molecular weight, higher quantum yield and exceptional two-photon action cross-section value of **C1Sn-2**, its biological imaging properties are attractive to explore. Consequently, the anticancer activities of complexes **C1Sn-1** and **C1Sn-2** were evaluated against three tumor cell lines (HepG2 (human hepatocellular liver carcinoma cell line), Hela (human cervical carcinoma cell line) and A549 (human pulmonary adenocarcinoma cell)) and one normal cell HELF (human embryonic lung fibroblast) using 3-(4,5-dimethyl-2-thiazolyl)-2,5-diphenyl-2-H-tetrazolium bromide assay. Cisplatin is a clinical anti-cancer drug, which was used as positive controls. Cisplatin is typically provided as a lyophilized powder in a vial containing 50 mg cisplatin, 450 mg NaCl, and 500 mg mannitol. When dissolved in 50 mL of water, this results in a 1 mg/mL solution (3.3 mmol/L) of cisplatin dissolved in 150 mmol/L saline. The IC_{50} results show that **C1Sn-2** displayed less invasive property (~64%, 10 μM, 24 h) in HELF cells, whereas a significant reduction in cell lines viability was detected. It is apparent that the IC_{50} value of **C1Sn-2** (~0.40%) possess more cytotoxicity for A549 than the commercial cisplatin (~10.22%) (see Table 1).

We therefore decided to evaluate the intracellular distribution of **C1Sn-2**. The A549 cells were incubated with 10 μM complex and ICT

Table 1
Inhibitory concentration IC_{50} (μM) of complexes C1, **C1Sn-1**, **C1Sn-2** and cisplatin against HepG2, Hela, A549 and HELF cells. Data were exhibited as the means ± standard deviations (SD).

Compounds	IC_{50} (μM)[a]			
	HepG2	Hela	A549	HELF
C1	10.70 ± 0.04	13.87 ± 0.03	14.01 ± 0.07	13.50 ± 0.07
C1Sn-1	4.16 ± 0.03	0.85 ± 0.04	2.15 ± 0.06	40.61 ± 0.03
C1Sn-2	3.98 ± 0.07	0.82 ± 0.05	0.40 ± 0.06	64.12 ± 0.09
Cisplatin	10.48 ± 0.04	11.37 ± 0.06	10.22 ± 0.03	16.93 ± 0.03

[a] Cells were incubated with C1, **C1Sn-1**, **C1Sn-2** and cisplatin for 24 h.

emission as well as 2P confocal micrographs in living cells were successfully achieved (Fig. 2a). Along with the incubation time, the two-photon fluorescence microscopy (2PFM) image indicates nuclear uptake of intense luminescence in the nucleus compared to other regions. To further confirm that the luminescence is in the nucleus, we co-stained **C1Sn-2** with the one known membrane-permeable DNA stains (Nuclear Red®), and tracked them by 2PFM. The almost complete overlay images clearly show the nuclear stain of **C1Sn-2** in the presence of Nuclear Red® (Pearson Correlation Coefficient Rr = 0.93). The three dimensional microscopy with higher spatial resolution also strongly suggested that **C1Sn-2** targeted intracellular nucleus (Fig. S8). In contrast, **C1** and **C1Sn-2** showed much less overlap with nuclear but strong overlap with cell cytoplasm (Fig. S9). To determine the possible mechanism of cell entry, A549 cells were incubated with 10 μM **C1Sn-2** for 30 min at 4 °C (Fig. S10), then washed and imaged directly. In this case, weak fluorescence was detected, highly indicating that **C1Sn-2** enters

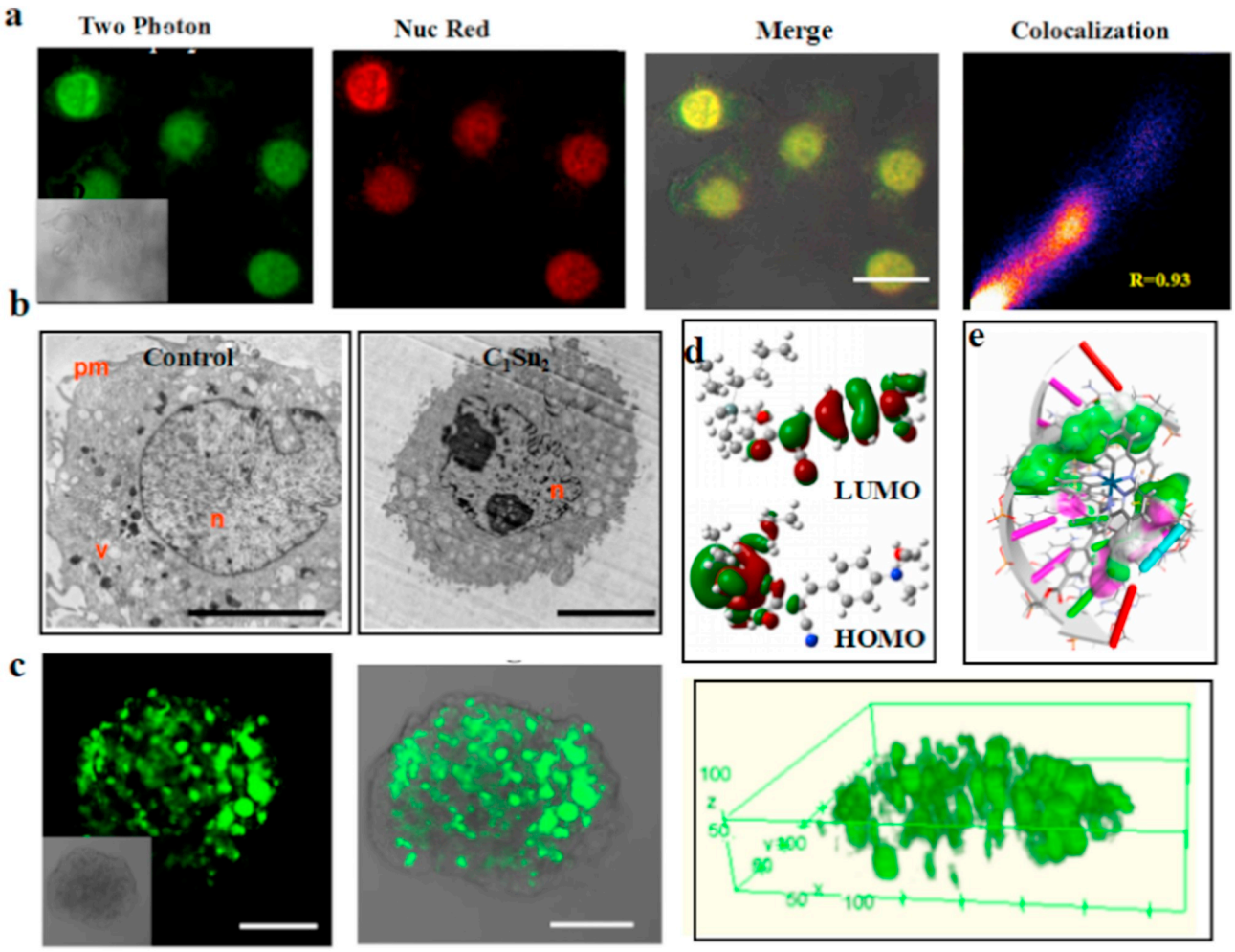

Fig. 2. (a)(1) Two-photon confocal micrograph of A549 cells incubation with 10 μM complexes **C1Sn-2** for continued irradiation 10 min, (2) Nuclear Red® stained A549 cells after incubated with **C1Sn-2** (10 μM), (3) Merge image and colocalization (Pearson's coefficients Rr = 0.93 (scale bar = 10 μm). (b) Transmission electron microscopy (TEM) microscopy of A549 cells stained with osmium tetroxide, solely incubated with **C1Sn-2** without osmium tetroxide; Abbreviations: n = nucleus. Transmission electron microscopy (TEM) (scale bar = 5 μm) (c) Two-photon fluorescence images of the 3D multicellular spheroids of A549 cells after incubation with 10 μM **C1Sn-2** for 5 h. (d) The frontier molecular orbitals distributions of **C1Sn-2** (e) Models obtained after molecular modeling of the interaction of **C1Sn-2** with DNA.

cells *via* a temperature-dependent pathway (*e.g.* endocytosis and active transport). We further evaluated the photo-physical stability in living cells (Fig. S11), the fluorescence intensity of **C1Sn-2** decreased to 97% while Nuclear Red® decreased to 19% after 350 s continued irradiation.

The two-photon fluorescence microscopy (2PFM) results highly demonstrated that **C1Sn-2** treated cell in nuclear region, which was in a good agreement with the IC_{50} results that **C1Sn-2** displayed a much stronger cytotoxicity response than **C1Sn-1**.

To confirm the localization that observed under confocal microscopy, transmission electron microscopy (TEM) experiments were performed to strengthen the above results. The cells here were incubated with **C1Sn-2** within 2 h incubation. It was clearly showed that OsO_4 treated cells co-treated with **C1Sn-2** contained abundant vacuoles, an organelle that plays a major role in early autophagy, leading to apoptotic cell death (Fig. 2b, left) [33]. In a good agreement with above confocal studies, it was also found that nucleus region beard much higher concentration, as well as displayed a certain degree of nucleus misshapen or damage (Fig. 2b right). The above Transmission electron microscopy (TEM) studies are in well agreement with the initial cell staining results exploited under confocal microscopy; further strengthen **C1Sn-2** targeted nucleus compartments with the anticancer effect.

2.4. Penetration ability in 3D MCSs

It is noteworthy that various anticancer drugs failed to penetrate into the monolayer cells to *in vivo* performance, partly due to the limitations of extracellular matrix (ECM). 3D multicellular spheroids (MCSs) as the tissue mode are widely applied in administration of drug delivery [34]. Hence, 200 μm 3D MCSs as the *in vivo* model were utilized to assess the therapeutic effect of **C1Sn-2**. To investigate the penetration ability, 200 μm A549 MCSs (Fig. 2c) were imaged incubating with 10 μM **C1Sn-2**. The results revealed that MCSs displayed remarkable fluorescence over 60 μm depth, suggesting that **C1Sn-2** could overcome ECM barrier and accumulate in MCS.

2.5. Nuclear targeting mechanism studies

The nuclear DNA fragmentation effect of **C1Sn-2** was confirmed by molecular modeling calculations using Gaussian and Discovery Studio Software [35]. The TD-DFT calculations (Fig. 2d) indicate that the high energy transition presents marked charge transfer (CT) character, with the HOMO being mainly located on triphenyltin hydroxide moiety and LUMO with moderate contribution from **C1** part, respectively. The docking results (Fig. 2e) indicate that **C1Sn-2** with suitable positive charge, lipophilicity and complex targeting moiety readily triggers DNA

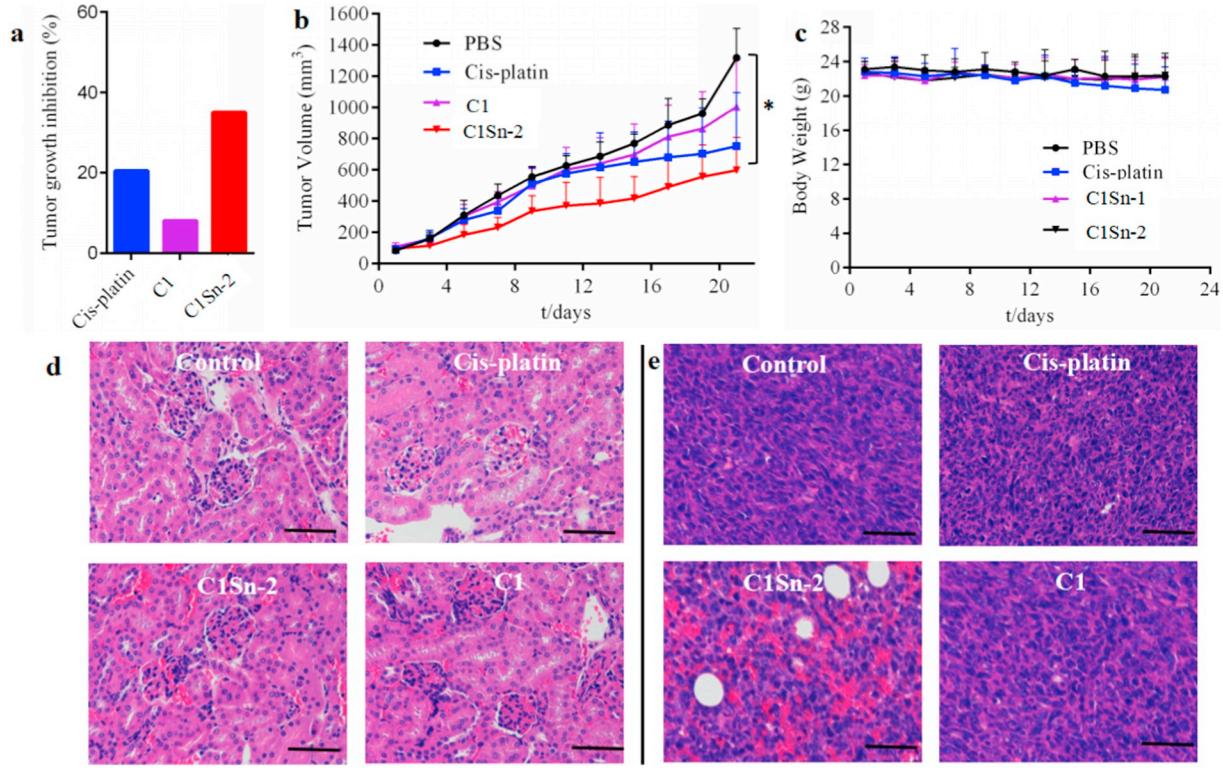

Fig. 3. (a) Growth inhibition rate of the solid tumor in the mice over 21 days under different treatment, (b) Tumor Volume under injection time point. (c) Body weight under different treatment over 21 days. (d) Kidney slices post-treatment with phosphate buffer saline (PBS), Cis-platin, **C1Sn-2** and C1. (e) Tumor slices (post-treated with PBS, Cisplatin, **C1Sn-2** and C_1, the tumors were extracted at 21st day. **C1Sn-2** (5 mg/kg) was injected intravenously. Scale bars = 100 μm.

through hydrogen bonds in different directions, which can stable with high Dock score and low CDOCKER energy. To further confirm that **C1Sn-2** was encapsulated by DNA, ^{1}H NMR titration experiments were carried out in d_6-DMSO-D_2O. A significant widen and low-field shifts of hydroxy protons Ha (Fig. S12) was occurred after 2 equiv. of DNA adding into **C1Sn-2** solution, demonstrating the presence of hydrogen bonds interactions between hydroxy group of **C1Sn-2** and DNA.

2.6. Flow cytometry analysis and anticancner effect

The IC_{50} of **C1Sn-2** of on A549 cells was 0.40 ± 0.06 μM and the possible mechanism of inducing cell death was investigated by annexin-V fluorescein isothiocyanate/propidium iodide (V-FITC/PI) double staining [36,37]. The late apoptotic/necrotic population (Annexin V +/PI−) of 10 μM **C1Sn-2** treated cells were increased from 2.79% to 66.79% by comparing with blank control (Fig. S13), whereas the viable of the untreated cells remained 97.21%. To further assess the anticancer effect, flow cytometry analysis was performed to investigate the cell cycle of A549 cells stained with PI (propidium iodide) in the presence of **C1Sn-2** (Fig. S14). After the treatment of complex **C1Sn-2**, the percentage of A549 cells in the P5 (G2M) phase decreased markedly from 19.26% to 15.58%, and there was a sharp increase of cells in the P3 (G0-G1) phase from 61.35% to 66.39% indicating that the cell cycle is arrested at the G0-G1 phase. (G2 phase follows the successful completion of S phase and prepares the cell for mitosis, consisting of protein synthesis and rapid cell growth. M phase is mitotic phase, which consists of nuclear division (karyokinesis)). The results indicated that **C1Sn-2** can significantly induce cell death *via* apoptosis/necrosis in low concentration.

Next, we investigated the anticancner effect of **C1Sn-2** in animal mode, Balb/C mice subcutaneous bearing 4 T1 tumors were intravenously injected with PBS (20 μL), cisplatin [38] (5 mg/kg), **C1Sn-2** (5 mg/kg) and **C1** (5 mg/kg) every four days for four times. The tumor growth of mice treated with **C1Sn-2** was significantly inhibited ($P < 0.05$). The tumor growth inhibition (TGI) of **C1Sn-2** group was 35.13% which was higher than the TGI 20.53% of cis-platin treated group (Fig. 3a). The volume of tumor treated with **C1Sn-2** is smaller from that treated with PBS which suggested that **C1Sn-2** displayed certain damage towards both cancerous cells and tumor in mice (Fig. 3b). Furthermore, no obvious body weight changes were detected after treatment of **C1Sn-2** (Fig. 3c). Body weight of the mice treated with cis-platin was decreased, indicating the toxicity of such chemotherapy agent. Study of the histological sections was demonstrated the renal toxicity of cis-platin by inducing inflammation. In the contrary, **C1Sn-2** showed non-obvious histological changes in the main kidney organs with non-significant toxicity (Fig. 3d). Necrosis and apoptotic regions were also presented in both control and cisplatin staining tumor tissue sections (Fig. 3e) from groups treated with **C1Sn-2**. These results suggested that **C1Sn-2** displayed a certain anti-cancer efficacy in animal mode with non-significant toxicity in the preliminary study.

3. Conclusion

In summary, two novel organotin complexes (**C1Sn-2** and **C1Sn-2**) were designed and synthesized and their photophysical properties were investigated systematically. The nonlinear optical (NLO) studies demonstrated that **C1Sn-2** possessed 2PA cross section (1107 GM) in near-IR range. Particularly, with slightly modification on terminal substitute, **C1Sn-2** was targeting to nucleus, and **C1Sn-1** targeted cytoplasm, respectively. The *in vitro* binding assay, two-photon fluorescence microscopy (2PFM) and transmission electron microscopy elucidated that **C1Sn-2** binds with nuclear DNA through H-bond in live cells. As expected, **C1Sn-2** exhibited deep MCSs penetration, which are favor of efficient anticancer application. **C1Sn-2** was successfully applied as a solid tumor growth inhibitor as a two-photon anticancer agent. The animal results suggest that **C1Sn-2** is a safe and effective candidate to

apply cancer therapy. This work offers a dual functional organotin complex for two-photon anticancer agent and nuclear targeting which could have significant potentials in utilizing such complexes as biomedical candidates.

Acknowledgments

This work was supported by the National Natural Science Foundation of China (21501001, 51432001, 51672002, 21602003, 81503009 and 51772002), Postdoctoral Science Foundation of Anhui Province (2016B092), China Postdoctoral Science Foundation (2017M612050), the Natural Science Foundation of Anhui Province (1508085MB34), Anhui Provincial Natural Science Foundation of China (1708085MC68), and Anhui University Doctor Startup Fund (J01001962), the Higher Education Revitalization Plan Talent Project (2013).

Appendix A. Supplementary data

Supplementary data to this article can be found online at https://doi.org/10.1016/j.jinorgbio.2018.12.001.

References

[1] R.D. Schreiber, L.J. Old, M.J. Smyth, Cancer immunoediting: integrating immunity's roles in cancer suppression and promotion, Science 331 (2011) 1565–1570.
[2] R. Hajek, J. Vorlicek, M. Slavik, Paclitaxel (taxol): a review of its antitum or activity in clinical studies minireview, Neoplasma 43 (3) (1996) 141–154.
[3] S. Dilruba, G.V. Kalayda, Platinum-based drugs: past, present and future, Cancer Chemother. Pharmacol. 77 (6) (2016) 1103–1124.
[4] H. Mukai, K. Kato, T. Esaki, S.Z. Ohsumi, Y. Hozomi, N. Matsubara, T. Hamaguchi, Y. Matsumura, R. Goda, T. Hirai, Y. Nambu, Phase I study of NK105, a nanomicellar paclitaxel formulation, administered on a weekly schedule in patients with solid tumors, Investig. New Drugs 34 (2016) 750–759.
[5] S.A.S. Syed, S. Muhammad, W. Amir, M. Ahmed, N. Tayyaba, S. Salma, R. Gildardo, Synthesis and biological activities of organotin(IV) complexes as antitumoral and antimicrobial agents. A review, Mini-Rev. Med. Chem. 15 (5) (2015) 406–426.
[6] M. Martins, P.V. Baptista, A.S. Mendo, C. Correia, P. Videira, A.S. Rodrigues, J. Muthukumaran, T. Santos-Silva, A. Silva, M.F.C. Guedes Da Silva, J. Gigante, A. Duarte, M. Gajewska, A.R. Fernandes, *In vitro* and *in vivo* biological characterization of the anti-proliferative potential of a cyclic trinuclear organotin(IV) complex, Mol. BioSyst. 12 (3) (2016) 1015–1023.
[7] S. Muhammad, A. Saqib, Organotin(IV) carboxylates as promising potential drug candidates in the field of cancer chemotherapy, Curr. Pharm. Des. 22 (44) (2016) 6665–6681.
[8] D.B. Shpakovsky, C.N. Banti, E.M. Mukhatova, Y.A. Gracheva, V.P. Osipova, N.T. Berberova, D.V. Albov, T.A. Antonenko, L.A. Aslanov, E.R. Milaeva, S.K. Hadjikakou, Synthesis, antiradical activity and *in vitro* cytotoxicity of novel organotin complexes based on 2,6-di-*tert*-butyl-4-mercaptophenol, Dalton Trans. 43 (2014) 6880–6890.
[9] Y. Yan, J.Y. Zhang, L.X. Ren, C.B. Tang, Metal-containing and related polymers for biomedical applications, Chem. Soc. Rev. 45 (2016) 5232–5263.
[10] F.F. Yan, C.L. Ma, Q.L. Li, S.L. Zhang, J. Ru, S. Cheng, R.F. Zhang, Syntheses, structures and anti-tumor activity of four organotin(IV) dicarboxylates based on (1, 3, 4-thiadiazole-2, 5-diyldithio) diacetic acid, New J. Chem. 42 (2018) 11601–11609.
[11] T.S.B. Baul, D. Dutta, A. Duthie, B.G.M. Rocha, M.F.C.G. da Silva, S. Saurav, S.K. Manna, Syntheses, structural snapshots, solution redox properties and cytotoxic performances of designated ferrocence scaffolds appended with organostannyl (IV) benzoates en route for human hepatic carcinoma, Organometallics 36 (2) (2017) 490–497, https://doi.org/10.1021/acs.organomet.8b00278.
[12] J. Magano, J.R. Dunetz, Large-scale applications of transition metal-catalyzed couplings for the synthesis of pharmaceuticals, Chem. Rev. 111 (2011) 2177–2250.
[13] K.D. Nolf, S.M. Cosseddu, J.J. Jasieniak, E. Drijvers, J.C. Martins, I. Infante, Z. Hens, Binding and packing in two-component colloidal quantum dot ligand shells: linear versus branched carboxylates, J. Am. Chem. Soc. 139 (9) (2017) 3456–3464.
[14] Q.H. Yang, Q. Xu, H.-L. Jiang, Metal–organic frameworks meet metal nanoparticles: synergistic effect for enhanced catalysis, Chem. Soc. Rev. 46 (2017) 4774–4808.
[15] B. Boitrel, I. Hijazi, T. Roisnel, K. Oohora, T. Hayashi, Iron-strapped porphyrins with carboxylic acid groups hanging over the coordination site: synthesis, X-ray characterization, and dioxygen binding, Inorg. Chem. 56 (13) (2017) 7373–7383.
[16] R.M. O'Donnell, R.N. Sampaio, G.C. Li, P.G. Johansson, C.L. Ward, G.J. Meyer, Photoacidic and photobasic behavior of transition metal compounds with carboxylic acid group(s), J. Am. Chem. Soc. 138 (2016) 3891–3903.
[17] L. Zhu, X.Q. Liu, H.-L. Jiang, L.-B. Sun, Metal–organic frameworks for heterogeneous basic catalysis, Chem. Rev. 117 (12) (2017) 8129–8176.
[18] I. Chakraborty, T. Pradeep, Atomically precise clusters of Noble metals: emerging link between atoms and nanoparticles, Chem. Rev. 117 (12) (2017) 8208–8271.
[19] M. Gielen, Review: organotin compounds and their therapeutic potential: a report from the organometallic Chemistry Department of the Free University of Brussels, Appl. Organomet. Chem. 16 (2002) 481–494.
[20] M.L. Sun, B.F. Ruan, Q. Zhang, Z.D. Liu, S.L. Li, J.Y. Wu, B.K. Jin, J.X. Yang, S.Y. Zhang, Y.P. Tian, Synthesis, crystal structures, electrochemical studies and antitumor activities of three polynuclear organotin(IV) carboxylates containing ferrocenyl moiety, J. Organomet. Chem. 696 (2011) 3180–3185.
[21] X.S. Zhao, J. Liu, H. Wang, Y. Zou, S.L. Li, S.Y. Zhang, H.P. Zhou, J.Y. Wu, Y.P. Tian, Synthesis, crystal structures and two-photon absorption properties of triphenylamine cyanoacetic acid derivative and its organooxotin complexes, Dalton Trans. 44 (2015) 701–709.
[22] H. Wang, L. Hu, W. Du, X.H. Tian, Q. Zhang, Z.J. Hu, L. Luo, H.P. Zhou, J.Y. Wu, Y.P. Tian, Two-photon active organotin (IV) carboxylate complexes for visualization of anticancer action, ACS Biomater Sci. Eng. 3 (5) (2017) 836–842.
[23] M. Nath, S. Pokharia, R. Yadav, Organotin (IV) complexes of amino acids and peptides, Coord. Chem. Rev. 215 (2001) 99–149.
[24] G.L. Law, C. Man, D. Parker, J.W. Walton, Observation of the selective staining of chromosomal DNA in dividing cells using a luminescent terbium(III)complex, Chem. Commun. 46 (2010) 2391–2393.
[25] M. Sirajuddin, S. Ali, V. McKee, S. Zaib, J. Iqubal, Organotin (IV) carboxylate derivatives as a new addition to anticancer and antileishmanial agents: design, physicochemical characterization and interaction with Salmon sperm DNA, RSC Adv. 4 (2014) 57505–57521.
[26] D. Chen, Y. Pan, L. Wang, Z.B. Zeng, L. Yuan, X.B. Zhang, Y.T. Chang, Selective visualization of the endogenous peroxynitrite in an inflamed mouse model by a mitochondria-targetable two-photon ratiometric fluorescent probe, J. Am. Chem. Soc. 139 (1) (2017) 285–292.
[27] W.B. Hu, M. Xie, H. Zhao, Y.F. Tang, S. Yao, T.C. He, C.X. Ye, Q. Wang, X.M. Lu, W. Huang, Q.L. Fan, Nitric oxide activatable photosensitizer accompanying extremely elevated two-photon absorption for efficient fluorescence imaging and photodynamic therapy, Chem. Sci. 9 (2018) 999–1005.
[28] G. Xu, S. Zeng, B. Zhang, M.T. Swihart, K.T. Yong, P.N. Prasad, New generation cadmium-free quantum dots for biophotonics and nanomedicine, Chem. Rev. 116 (19) (2016) 12234–12327.
[29] J.G. Jia, Y. Zhang, M. Zheng, C.F. Shan, H.C. Yan, W.Y. Wu, X. Gao, B. Cheng, W.S. Liu, Y. Tang, Functionalized Eu(III)-based nanoscale metal-organic framework to achieve near-IR-triggered and -targeted two-photon absorption photodynamic therapy, Inorg. Chem. 57 (2018) 300–310.
[30] Q. Zhang, X. Tian, Z. Hu, C. Brommesson, J. Wu, H. Zhou, S. Li, J. Yang, Z. Sun, Y. Tian, A series of Zn(II) terpyridine complexes with enhanced two-photon-excited fluorescence for in vitro and in vivo bioimaging, J. Mater. Chem. B 3 (2015) 7213–7221.
[31] B.-Z. Zhu, X.-J. Chao, C.-H. Huang, Y. Li, Delivering the cell-impermeable DNA 'light-switching' Ru(II) complexes preferentially into live-cell nucleus *via* an unprecedented ion-pairing method, Chem. Sci. 7 (2016) 4016–4023.
[32] P. Paitandi, S. Mukhopadhyay, R.S. Singh, V. Sharma, S.M. Mobin, D.S. Pandey, Anticancer activity of iridium(III) complexes based on a pyrazole-appended quinoline-based BODIPY, Inorg. Chem. 56 (2017) 12232–12247.
[33] N. Mizushima, Autophagy: process and function, Genes Dev. 21 (2007) 2861–2873.
[34] J.P. Liu, Y. Chen, G.Y. Li, P.Y. Zhang, C.Z. Jin, L.L. Zeng, L.N. Ji, H. Chao, H. Ruthenium, (II) polypyridyl complexes as mitochondrial-targeted two-photon photodynamic anticancer agents, Biomaterials 56 (2015) 140–153.
[35] G. Wu, D.H. Robertson, C.L. Brooks, M. Vieth, Detailed analysis of grid-based molecular docking: a case study of CDOCKER-A CHARMm-based MD docking algorithm, J. Comput. Chem. 24 (2003) 1549–1562.
[36] B. Schutte, R. Nuydens, H. Geerts, F. Ramaekers, Annexin V binding assay as a tool to measure apoptosis in differentiated neuronal cells, J. Neurosci. Methods 86 (1998) 63–69.
[37] I. Vermes, C. Haanen, H.S. Nakken, C. Reutelingsperger, A novel assay for apoptosis flow cytometric detection of phosphatidylserine expression on early apoptotic cells using fluorescein labelled Annexin V, J. Immunol. Methods 184 (1995) 39–51.
[38] D.B. Shpakovsky, C.N. Banti, E.M. Mukhatova, Y.A. Gracheva, V.P. Osipova, N.T. Berberova, D.V. Albov, T.A. Antonenko, L.A. Aslanov, E.R. Milaeva, S.K. Hadjikakou, Synthesis, antiradical activity and *in vitro*cytotoxicity of novel organotin complexes based on 2,6-di-*tert*-butyl-4-mercaptophenol, Dalton Trans. 43 (2014) 6880–6890.